

Synthesis of a novel amorphous metal organic framework with hierarchical porosity for adsorptive gas separation

Javier Fonseca ^{*}, Sunho Choi ^{**}

Department of Chemical Engineering, Northeastern University, 313 Snell Engineering Center, 360 Huntington Avenue, Boston, MA, 02115-5000, United States



ARTICLE INFO

Keywords:

Amorphous MOF
Hierarchical porosity
Amine loading
CO₂ adsorption

ABSTRACT

A novel amorphous iron metal-organic framework (NEU-2 = Fe(BPDI)(Py)₂, BPDI = N,N'-bis(glycinyl)pyromellitic diimide; Py = pyridine) with multichannel pore systems is synthesized, and subsequently tested as class 1 sorbent by evaluating its CO₂ capture capacity. Whereas the meso- and macro-pores present in NEU-2 are loaded with poly(ethylenimine) (PEI), micropores are maintained accessible for CO₂ diffusion. Tests at different temperatures and cyclic adsorption-desorption experiments are performed to examine CO₂ uptake and amine efficiency evolution. Moreover, the diffusion resistance present within the pores of the material is measured by comparing the fast uptake at the beginning of the capture (pseudo-kinetic regime) to the slow uptake at the end of capture towards equilibrium (pseudo-diffusive regime). It is also reported a comparative study of the CO₂ capture capacity of amorphous NEU-2 and crystalline NEU-1c. This research demonstrates that the ordered crystalline state of MOFs is not a requirement for gas uptake, establishing novel amorphous MOFs with hierarchical porosity as promising materials for CO₂-capture applications. It is evidenced that amorphous MOFs may facilitate a variety of chemical separations due to its framework flexibility and, ultimately, its guest-responsive capability.

1. Introduction

The continuously increasing CO₂ emissions from anthropogenic sources contribute enormously to the greenhouse gas effect and global warming. The United States Environmental Protection Agency reported that the impact of anthropogenic gases on climate change increased by approximately 37% from 1990 to 2015 [1]. In addition, the Earth's average temperature has been shown to have risen approximately 0.8 °C since 1880, and 0.15–0.20 °C per decade since 1975 [2]. Many efforts have been made to fulfil the necessity for effective CO₂ capture over the past decades. A wide range of CO₂ capture technologies have been considered, including absorption [3–5], adsorption [6–8], membrane technology [9,10], and cryogenic distillation [11]. Currently, liquid amine scrubbing is the most mature technology for CO₂ sorption. This process is widely used by the petrochemical industry on large scales to separate CO₂ from gas streams. However, traditional amine scrubbing methods suffer from high regeneration energy consumption, limited absorption capacity, low thermal and oxidation stability, high volatility, high corrosive and toxic nature, and generation of unpleasant by-products [12]. It must be noted that diamines allow higher CO₂

loading capacity than conventional monoethanolamine (MEA) absorbent: the additional NH group in diamine provides further sites for chemisorption of CO₂ molecules [13]. On the other hand, solid sorbents present superior adsorption performance and kinetics in addition to low regeneration energy. Depending on the adsorption temperature range, solid sorbents can be classified as high-temperature, mid-temperature, or low-temperature sorbents, such as CaO-based sorbents, K₂CO₃, and metal-organic frameworks (MOFs), respectively [14].

Hybrid sorbents based on porous materials such as zeolites, MOFs, and porous carbon that are doped with amine are promising alternatives for CO₂ capture. These hybrid sorbents combine the advantages of physisorption and chemisorption. Amine-based sorbents are commonly classified depending on how amines are located within the sorbent. When amines are chemically attached to pore walls, amine-based sorbents are considered as class 2 and 3 sorbents. Conversely, class 1 are those hybrid sorbents in which amines only interact physically with the pore walls [15]. Usually, this class of hybrid sorbents are developed by the immobilization of amine via wet-impregnation method followed by drying in a high surface area and high pore volume sorbent [16]. Recently, freeze-drying methods have been reported to incorporate

* Corresponding author.

** Corresponding author.

E-mail addresses: fonsecagarcia.j@northeastern.edu (J. Fonseca), s.choi@northeastern.edu (S. Choi).

amine while also maintaining the integrity of the mesoporous silica structure – CO₂ sorption capacity was around 18 times higher than the analogue sorbents prepared by the drying method [17].

Class 1 sorbents have been created with a wide variety of mesoporous materials [18–20]. However, these material-based class 1 amine sorbents present drawbacks. The amine loading is restricted to the mesopore space, thus limiting adsorption capacity. Moreover, CO₂ diffuses deficiently to internal amine sites due to lack of accessible open pores. This diffusional limitation reduces CO₂ uptake capacities and kinetics. In addition, amines easily clog and fill small mesoporous channels. Materials with hierarchical porosity can potentially address these challenges. While micro- and small mesoporous regimes facilitate CO₂ diffusion, large meso- and macroporous channels provide space for loading high amine cargoes [15]. In this work, we synthesized a new hierarchical amorphous MOF (aMOF) and examined, for the first time, the potential of aMOFs as class 1 sorbent by evaluating its CO₂ capture capacity.

Crystalline MOFs are coordination networks in which inorganic nodes (clusters or metal ions) are linked by organic ligands. These frameworks define an infinite array of crystal units that has potential for high porosity and display long-range order. The synthesis of MOFs has been intensively investigated over the past decade due to their potential in gas storage and separation, catalysis, drug delivery and sensing applications. To date, more than 60,000 crystalline MOFs structures have been identified. Additionally, scientific interest in non-crystalline systems with similar metal-ligand bonding motifs to their crystalline counterparts is growing. aMOFs are networks of inorganic nodes connected by organic ligands in either two or three dimensions with potential for porosity, displaying no long-range order within the structure. Thus, aMOFs retain the basic building blocks and connectivity of their crystalline cousins but exhibit only diffuse scattering from X-ray or neutron diffraction. Even though aMOFs offer many opportunities for practical application, this domain is largely unexplored and just a small number (fewer than 200) of porous aMOFs have been reported [21–23].

aMOFs have mostly been prepared by introducing disorder into initial crystalline frameworks through heating [24–35], pressure (both hydrostatic and nonhydrostatic) [36–45], electrical discharge [46], and ball-milling [47–51]. A few aMOFs have been formed by direct synthesis of a metal node and organic ligand [52–54]. To the best of our knowledge, only 15 directly synthesized aMOFs have been reported to exhibit porosity (Table 1) [55–64]. aMOFs can also be produced upon solvent removal [65], but the chemical composition changes between the crystalline and amorphous forms of MOFs during this procedure. It must be noted that MOF glasses can be formed by melt quenching through rapid cooling, which avoids crystallization of a liquid [66–70]. aMOFs

Table 1
Directly synthesized aMOFs with permanent porosity.

Sample name	BET surface area (m ² g ⁻¹)	Ref.
NEU-2	220.9	This work
a-Fe ^(III) ₃ O(C ₆ H ₃ (COO) ₃) ₂ NO ₃	1618	[55]
a-Zn(ICA)-2	251	[56]
a-Fe ₃ Ni ₂ (BDC-NH ₂)	142.2	[57]
a-FMM-120	42.6	[58]
CPPs-1	584.7	[59]
CPPs-3	522.4	
CPPs-5	587.5	
a-Ni-pPD	35	[60]
a-Zr-MOF(23)	410	[61]
a-Zr-MOF(24)	955	
a-Zr-MOF(25)	535	
a-Zr-MOF(26)	546	
a-[Ru(C ₅ H ₅) ₂ B(CN) ₄] _n	80–202	[62]
a-Ni ⁺⁺ -1,3,5-tribenzyl-1,3,5-triazine-2,4,6-(1H,3H,5H)-trione	3181	[63]
a-CoL NL	105.7	[64]

combine both the versatility of MOF chemistry and the attractive properties of amorphous materials such as hierarchical porosity. An array of materials displaying unique chemical and physical properties is expected to emerge by moving away from crystalline MOFs. aMOFs are only starting to be applied over multiple areas including harmful species detection [71], drug delivery [34,50], gas storage [45], radioisotopes storage [39,49], water treatment [59], and catalysis [30,33].

In this research, a novel amorphous iron MOF (NEU-2) with multi-channel pore systems was created and tested for the first time as class 1 sorbent by evaluating its CO₂ capture capacity, demonstrating that the ordered crystalline state is not a requirement for gas uptake. PEI-loaded NEU-2 (NEU-2-PEI) was prepared by incorporating large PEI molecules preferentially into the meso- and macroporous present in NEU-2. NEU-2-PEI enables open micropores to be accessible for CO₂ diffusion to internal amine sites; in other words, NEU-2-PEI allows amine loading with access to amine sites. The changes in CO₂ capture capacity at equilibrium and the amine efficiency of NEU-2-PEI are tested at increasing amine loadings. In addition, tests at different temperatures and cyclic adsorption-desorption experiments were performed to examine CO₂ uptake and amine efficiency evolution. Herein, it is also reported a comparative study of the CO₂ capture capacity of amorphous NEU-2 and crystalline NEU-1c. It is shown that crystalline forms are not a prerequisite for gas uptake.

2. Experimental section

2.1. Chemicals and materials

Glacial acetic acid (C₂H₄O₂, 99.7%), 1,2,4,5-benzenetetracarboxylic anhydride (C₁₀H₂O₆, 99%), glycine (C₂H₅NO₂, crystalline), zinc acetate dihydrate (C₄H₁₀O₆Zn, crystalline), pyridine (C₅H₅N, 99%), 2-methyltetrahydrofuran (C₅H₁₀O, >99%), and methanol (CH₃OH, ≥99.8%) were purchased from Fisher Scientific. Iron (II) acetate anhydrous (Fe (OOCH₃)₂, Fe 29.5% min) was acquired from Alfa Aesar. Polyethylenimine, branched (H(NHCH₂CH₂)_nNH₂, 99%) was purchased from Sigma Aldrich. All the materials were used as-received without further purification.

2.2. Characterization

NEU-1c and NEU-2 were characterized by powder X-ray diffraction (PXRD) using a Rigaku (model Ultima IV) diffractometer with Cu K α radiation ($\lambda = 1.5418 \text{ \AA}$) at 40 kV and 40 mA. Nuclear magnetic resonance (NMR) characterization of H₂BPDI ligand (¹H NMR) was carried out on a Varian Unity Inova 500 MHz spectrometer. Fourier-transform infrared spectroscopy (FTIR) spectra were performed using a Shimadzu FTIR with a wavenumber range of 500–4000 cm⁻¹. Differential scanning calorimetry (DSC) characterization of H₂BPDI material was carried out on a TA instrument DSC 250. H₂BPDI was heated from 40 to 400 °C at a rate of 1 °C min⁻¹ under a nitrogen flow. Scanning Electron Microscopy (SEM) was performed on a Hitachi S-4800. Energy-dispersive X-ray spectroscopy (EDX) spectroscopy analysis was performed using a dedicated EDX detector coupled with a Hitachi S-4800 SEM. An accelerating voltage of 10 kV was used to obtain an elemental spectrum of NEU-2. Transmission Electron Microscopy (TEM) images were taken with a JEM-1010 (JEOL, Tokyo, Japan). Nitrogen adsorption/desorption isotherms of NEU-1c and NEU-2 were collected using a Quantachrome NOVA 2200e Series. Pore and surface analysis (BET surface area, BJH pore size and volume, and other surface and porosity data) was determined using the NOVA Win software. Prior to the measurements, the adsorbent was outgassed at 373 K under dynamic vacuum for 4 h. Thermogravimetric analysis (TGA) was performed to NEU-2 as well as NEU-1-PEI(x%wt) and NEU-2-PEI(x%wt) samples by using a TA instrument TGA Q500 in which samples were heated from room temperature to 600 °C at a rate of 5 °C min⁻¹ under a nitrogen flow. The *ex situ* X-ray absorption (XAS) studies were performed at the 7-ID

beamline of the National Synchrotron Light Source (NSLS) II (Brookhaven National Laboratory).

2.3. Preparation of *N,N*-bis(glycinyl)-pyromellitic diimide (H_2BPDI)

N,N-bis(glycinyl)-pyromellitic diimide (H_2BPDI) was synthesized with slightly modifications as previously reported [72,73]. Pyromellitic dianhydride (1.635 g, 7.5 mmol) was dissolved in glacial acetic acid (40 mL) by warming to 40 °C for 30 min. Finely powdered glycine (1.125 g, 15 mmol) was added to this solution and refluxed for 4 h. The resulting transparent, white solution was filtered and washed with de-ionized water several times. Finally, the solid was dried overnight in an oven at 70 °C. Yield: 1.75 g (5.3 mmol, 71%). 1H NMR (500 MHz, CD_3OD): δ 8.39 (s, 2H, ArH), 4.52 (s, 4H, $-CH_2-$) (Fig. S1). IR (KBr cm^{-1}): 3033 (O-H), 1784 (C=O), 1718 (C=O), 1409 (C-N), 1388 (C-N), 748 (C=O) (Fig. S2). H_2BPDI was also characterized with DSC (Fig. S3).

2.4. Synthesis of crystalline NEU-1c

NEU-1c was synthesized as reported in our previous publication [74]. Zinc acetate dihydrate (0.3293 g, 1.5 mmol) was dissolved in pyridine (1 mL) by sonication for 1 h. Similarly, H_2BPDI (0.3738 g, 1.126 mmol) was sonicated in 2-MeTHF (70 mL) for 1 h. Both solutions were combined on a Teflon-lined Parr reactor of 100 mL of capacity. The reaction mixture was solvothermally treated at 100 °C for 24 h. Yield: 0.4082 g. (Figs. S4–7).

2.5. Synthesis of amorphous NEU-2

Iron (II) acetate anhydrous (0.1582 g, 0.91 mmol) was dissolved in pyridine (1 mL) by sonication for 5 min. Similarly, H_2BPDI (0.1246 g, 0.375 mmol) was sonicated in 2-MeTHF (70 mL) for 1 h. Subsequently, both solutions were combined on a Teflon-lined Parr reactor of 100 mL capacity. The reaction mixture was solvothermally treated at 100 °C for 24 h. Yield 0.1523 g.

2.6. EXAFS analysis

The raw data was processed using the FEFFIT code and the Athena and Artemis interfaces of the Demeter software package [75]. The spectrum was energy-calibrated, merged and normalized. The EXAFS spectrum was extracted in k-space, Fourier-transformed on the range $k = 3.000\text{--}13.626 \text{ \AA}^{-1}$ and fitted in R-space between 1.0 and 4.2 Å for NEU-2 at the Fe K-edge. EXAFS modelling was carried out considering k^1 , k^2 and k^3 -weighting. Similarly, the EXAFS spectrum was extracted in k-space, Fourier-transformed on the range $k = 3.000\text{--}13.994 \text{ \AA}^{-1}$ and fitted in R-space between 1.0 and 4.4 Å for NEU-1c at the Zn K-edge. EXAFS modeling was also carried out considering k^1 , k^2 and k^3 -weighting.

2.7. Computational details

Calculations were carried out using the Amsterdam Density Functional (ADF 2019.102) program [76–78] on Gaussian geometries developed by Baerends et al. [76,77], and parallelized as well as linearized by Fonseca Guerra et al. [78].

The geometry of the local molecular structure of iron within NEU-2, has been fully optimized to a level that gives a good description of the electron density and orbital energies. Geometries, electron densities, and energies were calculated at the BP86 level of the generalized gradient approximation (GGA).

2.8. Amine impregnation

NEU-1c and NEU-2 samples were impregnated with polyethylenimine (PEI, branched 1800 MW) to create supported-amine

adsorbents. PEI was chosen due to its large molecular size. Around 0.2 g of support (NEU-1c and NEU-2), which was activated under vacuum for 4 h at 100 °C before impregnation, was added to varying amounts of PEI in methanol solution to form differing concentrations of support to PEI-solution. This solution was stirred vigorously for 2 h at room temperature. After impregnation, the sample was collected via washing with methanol, followed by vacuum filtration and further drying overnight at 60 °C. Samples were named as NEU-1-PEI(x%wt) and NEU-2-PEI(x%wt), where x is the weight percent of polymer loaded as determined by thermogravimetric analysis (Fig. S11). For instance, NEU-2 with a 3.23 wt% of polymer is named NEU-2-PEI(3.23%wt).

2.9. CO_2 capture performance

CO_2 capture trials were performed via TGA. A small amount of sample (~10–35 mg) was placed in a platinum sample pan. The system was equilibrated at 25 °C under a pure nitrogen flow, after which the sample was heated to 100 °C at a rate of 5 °C min⁻¹. This temperature was held for 180 min to desorb species adsorbed from air without damaging the impregnated amines. The system was then cooled back to 25 °C and held under nitrogen flow at this temperature for 60 min. Then, the gas was switched to a pure CO_2 stream to perform CO_2 capture at 25 °C for 600 min. The weight gain during the adsorption step was then analyzed to determine the CO_2 adsorption capacity values (pseudo-equilibrium capacity).

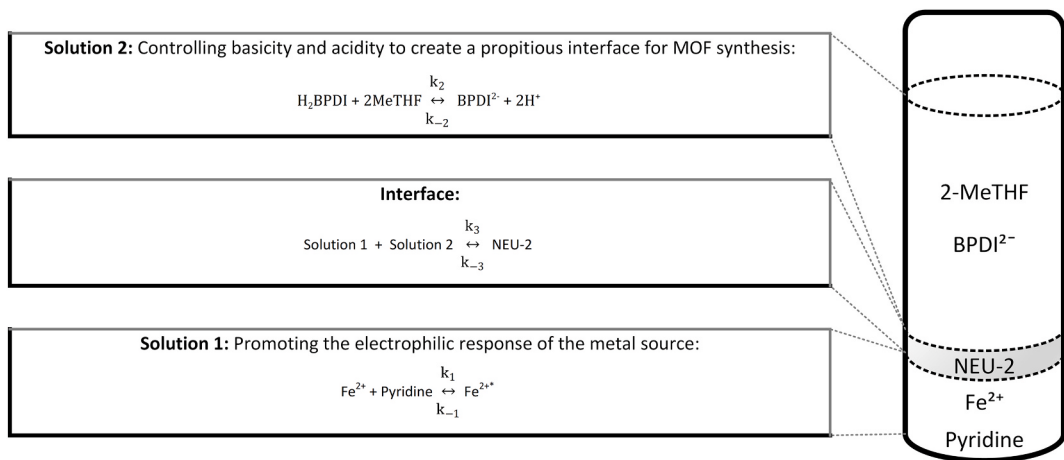
The amine efficiency (moles of CO_2 captured per moles of N present on the amine) was achieved on NEU-2-PEI(x%wt). The weight percent of the amine-containing molecules was converted into the molar content of nitrogen groups and compared to the capacity of carbon dioxide captured. All amine groups present on the impregnated PEI were assumed to be equally capable of capturing CO_2 .

3. Results and discussion

3.1. Preparation and characterization of NEU-2

The novel amorphous iron MOF ($Fe(BPDI)Py_2$ = NEU-2) was created by applying our recently reported liquid-liquid interface synthesis method [74]. NEU-2 was synthesized by using a high electron-donating solvent (pyridine) and a complementary co-solvent (2-methyl-tetrahydrofuran = 2-MeTHF) to cushion basicity (Scheme 1). The electrophilic behavior of Fe^{2+} was stimulated with pyridine. Thus, the electron transfer from the open-shell ligand ($BPDI^{2-}$) to Fe^{2+} was promoted. Pyridine solvent additionally acted as a capping ligand, blocking the MOF growth in one direction and, consequently, promoting the synthesis of the two-dimensional framework. The medium basicity was buffered with 2-methyl-tetrahydrofuran (2-MeTHF), thus creating a propitious interface to MOF synthesis. This buffering produced low connectivity of the linkers. 2-MeTHF also promoted the deprotonation of H_2BPDI and acted as a capping agent. Consequently, the reaction medium consists of two liquid regions (pyridine and 2-MeTHF solutions) that have low miscibility, separated by an intermediate region which displayed a pH around 4.34. Under static conditions, Fe^{2+} and $BPDI^{2-}$ are diffused into the transitional segment where nuclei are instantaneously developed. These nucleation sites are located close enough to each other for the formation of small crystalline domains.

The amorphous structure of NEU-2 was confirmed from the PXRD pattern as shown in Fig. 1a. This amorphous construction is a consequence of both the dynamic behavior of $BPDI^{2-}$, which created heterogeneity/disorder within NEU-2, and the function of 2-MeTHF as capping agent. The local molecular structure of iron within the MOF was determined via extended X-ray absorption fine structure (EXAFS) (Fig. 1b–f) (Fig. S8), together with DFT calculations. Near coordination shells were found to correspond to $Fe-N_1$ at $1.95620 \pm 0.06503 \text{ \AA}$ and $Fe-O_1$ at $1.96290 \pm 0.00089 \text{ \AA}$ with coordination number of 2 and 4, respectively (Table S1). Thus, secondary building units (SBUs) display



Scheme 1. Synthesis approach of NEU-2.

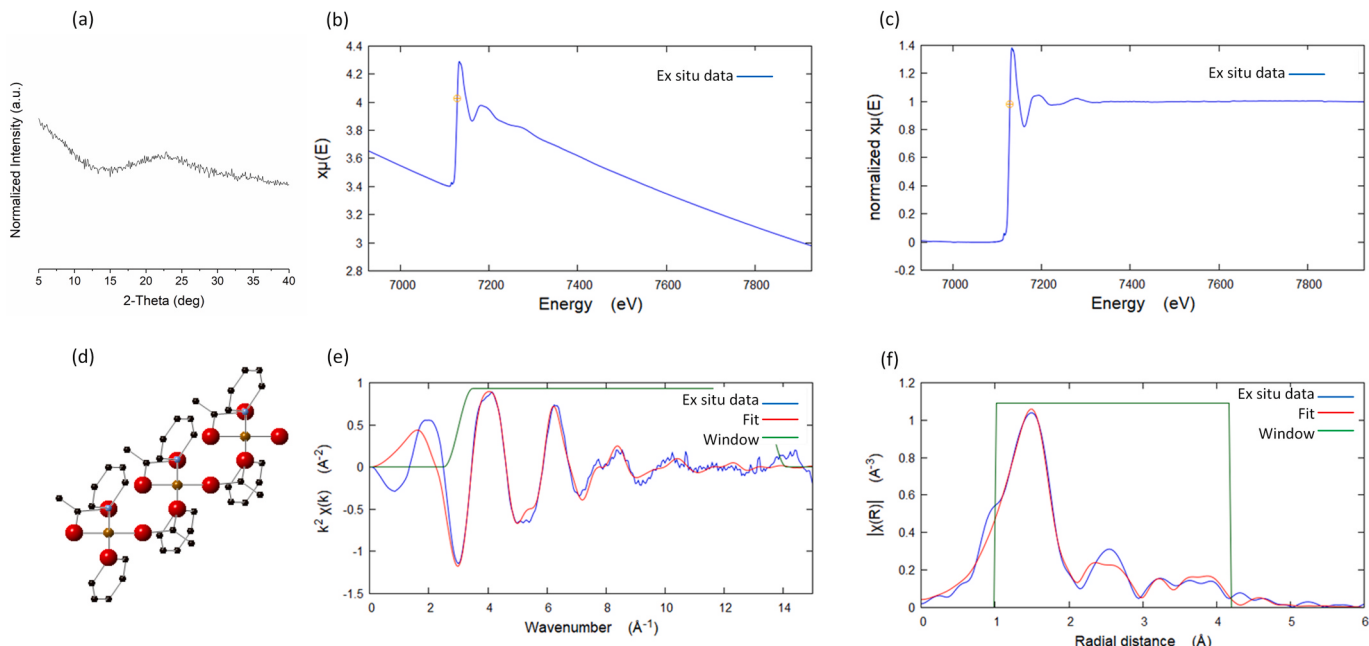


Fig. 1. (a) Powder X-ray (PXRD) diffractogram ($\text{Cu K}\alpha$ radiation) of NEU-2. (b) X-ray absorption spectrum at the Fe K-edge of the NEU-2 before (b) and after normalization (c). (d) Model of the local molecular structure of iron within NEU-2 ($\text{Fe}(\text{BPDI})\text{Py}_2$). Atom labelling scheme: C = black; O = red; N = blue; Fe = orange. H atoms are omitted for clarity. *Ex situ* Fourier transform extended X-ray absorption structure (FT-EXAFS) spectra at the Fe K-edge of the NEU-2 at both the K (e) and R (f) spaces, together with the corresponding EXAFS fittings. (For interpretation of the references to colour in this figure legend, the reader is referred to the Web version of this article.)

an octahedral coordination environment in NEU-2.

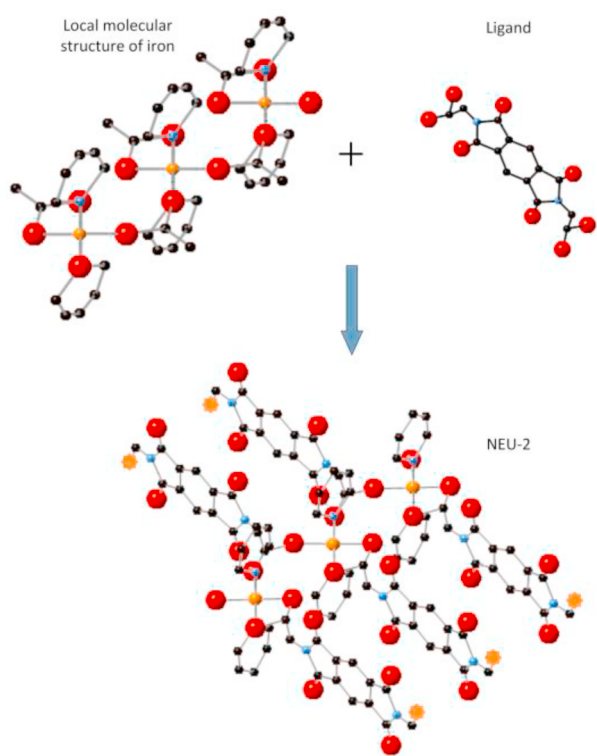
Outer coordination shells from 2.0 to 4.2 Å helped to determine the joining between SBUs, finding that H_2BPDI molecules coordinate to the equatorial plane. Each carboxylate group associated with the H_2BPDI molecule attaches differently to the iron metal. One carboxylate coordinates in a bidentate fashion, whereas the other two carboxylates coordinate to the metal in a monodentate fashion. In doing so, H_2BPDI molecule acts as a bridging ligand between the Fe atoms (Scheme 2).

In order to determine the elemental composition of NEU-2, EDX analysis was performed (Fig. S9). It showed the presence of iron (7.38 ± 1.13 wt%, 2.14 ± 0.31 m%) within the sample, as well as that of carbon (61.71 ± 4.91 wt%, 71.43 ± 5.71 m%), nitrogen (1.95 ± 1.53 wt%, 2.16 ± 2.37 m%) and oxygen (28.95 ± 5.72 wt%, 24.31 ± 4.31 m%). Weight and atomic content were determined in different zones and the average was calculated. SEM and TEM (Fig. 2) were performed to investigate the morphology of NEU-2. The result of both techniques showed

nanospheres of around 100 nm in diameter. This morphology is related to our previously reported material in which $\text{Zn}(\text{BPDI})(\text{Py})_2$ sheets self-organize into a three-dimensional supramolecular coordination material with spherical conformation (NEU-1) [74].

The thermal stability of NEU-2 was investigated from room temperature to 1000 °C at a rate of 5°C min^{-1} under a nitrogen flow by TGA (Fig. S10). NEU-2 showed a total mass loss of ~ 75.98 wt% on heating up to 1000 °C. The mass loss occurs in three steps: (1) mass loss of ~ 4.92 wt % at ~ 100 °C due to the desorption of trapped moisture, which is common in porous materials with a high surface area [79], (2) mass loss of ~ 37.82 wt% on heating up to ~ 350 °C due to the decomposition of ligated pyridine in axial position [80], (3) mass loss of ~ 22.09 wt% on heating up to 460 °C due to the decomposition of the remaining BPDI^{2-} ligands [74].

The porous nature of NEU-2 was evaluated by nitrogen adsorption/desorption measurements at 77 K (Fig. 3a). NEU-2 yielded an isotherm



Scheme 2. Reaction scheme for the synthesis of NEU-2.

which shows a type-2 curve, indicative of macroporous sorbents. In addition, the isotherm displayed a rapid uptake at low partial pressures, which indicated the presence of micropores and a large hysteresis loop in the mesopore regime. Therefore, NEU-2 may have a hierarchical pore distribution with the presence of micropores, mesopores, and macropores. DFT analysis of the pore size distribution provided complementary information about the multichannel distribution of NEU-2. Fig. 3b shows up to five different pore radii at 6.7 Å, 22.7 Å, 63.9 Å, 87.6 Å and 137.4 Å, thus confirming the presence of micro-, meso- and macroporosity in NEU-2. The BET surface area and total pore volume of NEU-2, which were calculated via the BJH analysis method, were found to be 220.9 m² g⁻¹ and 0.554 cm³ g⁻¹, respectively (Table 1).

3.2. NEU-2 as supported amine material for CO₂ adsorption

3.2.1. Effect of PEI loading

The potential of an aMOF (NEU-2) with hierarchical porosity as class 1 sorbent was tested for the first time by evaluating its CO₂ capture capacity, demonstrating that the ordered crystalline state is not a

requirement for gas uptake. NEU-2 was functionalized with polyethylenimine (PEI), a large amine polymer species. PEI was accommodated into the large mesopores and macropores present in NEU-2. The amine density within the system was increased to examine not only the variations in the CO₂ uptake capacity at equilibrium but also the capture capacity in the pseudo-kinetic and pseudo-diffusive regimes and the amine efficiency of the NEU-2-PEI. FTIR was used to assess the structural alterations in NEU-2 support due to amine impregnation (Fig. 4a). While the vibrational modes of NEU-2 (starting from the left: asymmetrical and symmetrical C=O stretching vibration of the imide at 1784 cm⁻¹ and 1718 cm⁻¹, respectively; imide C=O ring deformation at 1385 cm⁻¹; and imide C-H vibration at 748 cm⁻¹) are highlighted in blue, those vibrational modes of PEI (starting from the left: broad absorption peak of amine N-H stretching above 3000 cm⁻¹, C-H stretching at 2900 cm⁻¹ and N-H deformation at 1600 cm⁻¹) are depicted in yellow in Fig. 4a. The absorption frequency of the vibrational modes of NEU-2 were not altered, however, absorption intensity progressively decreased as amine impregnation content increased. The effects of pore filling of NEU-2, which may change how effectively the infrared photon energy is transferred to the molecule, could be a possible reason for the reduction in intensity. On the other hand, the vibrational modes of PEI quickly appeared with 1.35 wt% loading and the absorption intensity progressively increased as amine loading raised.

Morphological alterations in NEU-2 upon amine loading were tested by performing TEM. No change in the size or shape of the material was found due to the inclusion of PEI (Fig. S12). Therefore, the overall morphology of NEU-2 was maintained upon amine impregnation. The isotherm shifted to lower volumes of nitrogen adsorbed at low pressures upon amine loading, denoting loss of large meso- and macroporosity in NEU-2 due to the occupancy of PEI within the large meso- and macropores. The hysteresis loop of NEU-2-PEI was preserved as indicated by the shape maintaining. Therefore, PEI functionalization did not significantly alter mesopores (Fig. 3a). The pore space-PEI interactions in NEU-2 (Fig. 3b) is shown by the pore volume data obtained through DFT. The amount of large meso- and macropores decreases significantly upon PEI loading. Since PEI is too large to fit within the microporous, it can only be placed in the mesoporous and macroporous spaces. PEI will also sit along the outer surface of NEU-2, resulting in what appears to be a loss of microporosity. However, since gas diffusion proceeds quickly within the NEU-2-PEI systems (as it is shown in the CO₂ capture results), it suggests that amine groups are still accessible to entering CO₂ molecules, and therefore it is unlikely that the micropores are truly clogged by this large polymer. Instead, this result is due to the inability of the isotherm method to distinguish between filled microporous channels and channels with some source of diffusion resistance at the openings of the pore.

The surface area through the BET method and pore volume via the BJH analysis method were calculated from the isotherms (Table 2). Upon amine loading, the surface area of the MOF supports as well as the pore volume decreased significantly. Therefore, the bulk of the free

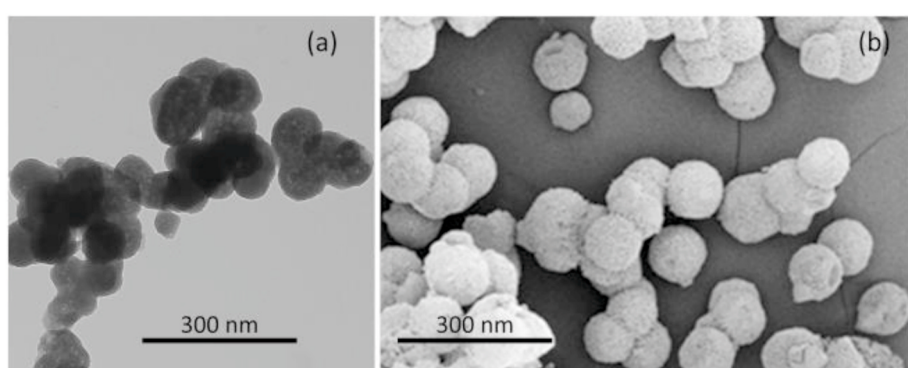


Fig. 2. TEM (a) and SEM (b) images of NEU-2.

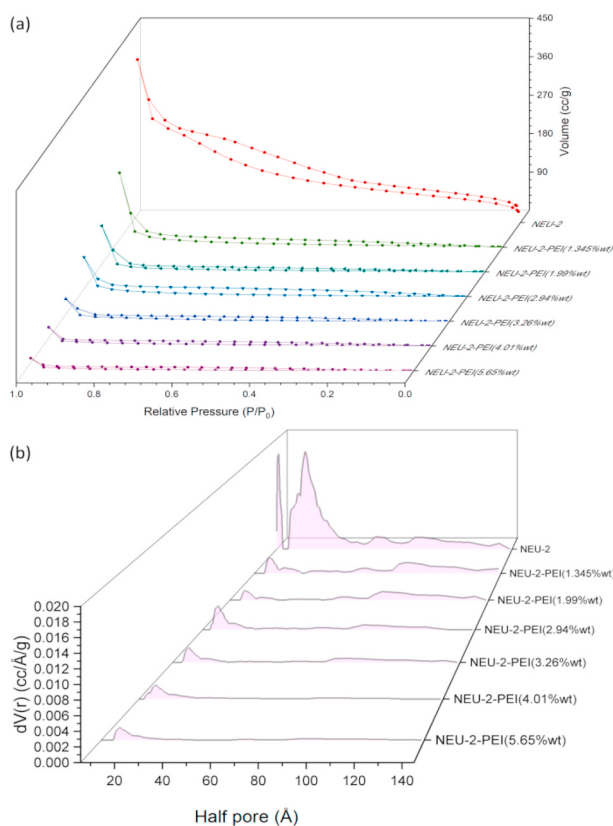


Fig. 3. (a) Nitrogen adsorption/desorption isotherms of NEU-2. (b) DFT pore analysis of NEU-2.

volume in the material is reduced due to the introduction of PEI primarily into the large pores and on the outer surface of NEU-2. On the other hand, it must be noted that the filling of one pore type over another will affect the accessibility of the other pore regions due to the non-uniform and complex pore channels in NEU-2.

The CO_2 capacity versus amine weight percent for NEU-2 and NEU-2-PEI is shown in Fig. 4b. NEU-2 support showed a CO_2 capture capacity of

0.1136 mmol g⁻¹ at room temperature in pure CO_2 . The sorbent showed an increase in CO_2 capture capacity upon impregnation with branched PEI from 0 wt% to 5.65 wt% of amine content. Therefore, the PEI loaded into the macro- and mesoporous allowed for the retention of the diffusion channels throughout the smallest mesopores and micropores present in NEU-2. Thus, the material did not show a significant loss of access through the pore channels upon PEI loading. Consequently, NEU-2 solves the conventional trade-off suffered by supported amine CO_2 -adsorbents between increasing amine content and decreasing access to amine sites.

The change in amine efficiency indicates how amines are being utilized for CO_2 capture and how effective amine loading is at improving capture capacity. It must be noted that the amine efficiency values tend to be overestimated by including both physically and chemically captured gas. Consequently, a calculated amine efficiency higher than 0.5 suggests that physical adsorption is the primary capture mechanism on the adsorbent. The efficiency was maintained with increasing amine content. Consequently, CO_2 was able to access available amine sites even at rising amine loadings.

It is also compared the CO_2 uptake capacity during the initial quick adsorption to the capacity obtained when diffusion resistance is dominant in order to test the changes to CO_2 diffusion through the sorbents.

Table 2
NEU-2 sorbent surface area and pore volume depending on the amine content.

Sample name	Amine loading (wt%)	BET surface area (m ² g ⁻¹)	Total pore volume (via BJH analysis method) (cc g ⁻¹)
NEU-2	0.00	220.9	0.554
NEU-2-PEI (1.35%)	1.35	16.8	0.274
NEU-2-PEI (1.99%)	1.99	10.5	0.169
NEU-2-PEI (2.94%)	2.94	9.0	0.148
NEU-2-PEI (3.26%)	3.26	7.6	0.138
NEU-2-PEI (4.01%)	4.01	5.1	0.086
NEU-2-PEI (5.65%)	5.65	3.4	0.048

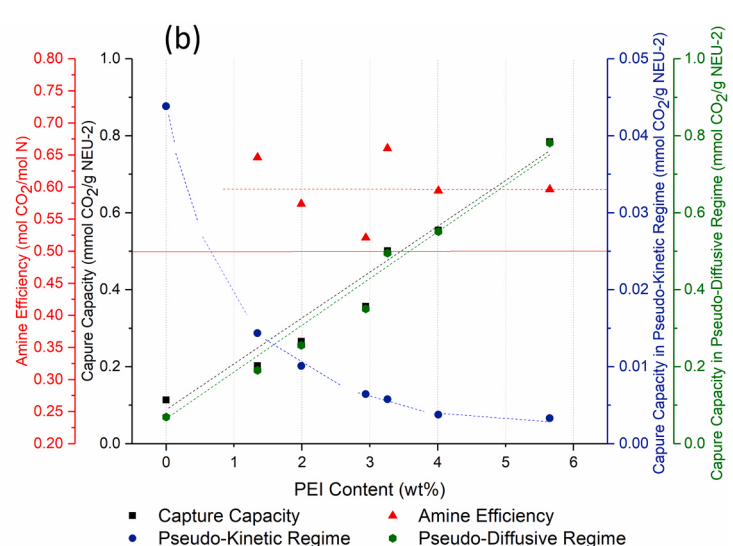
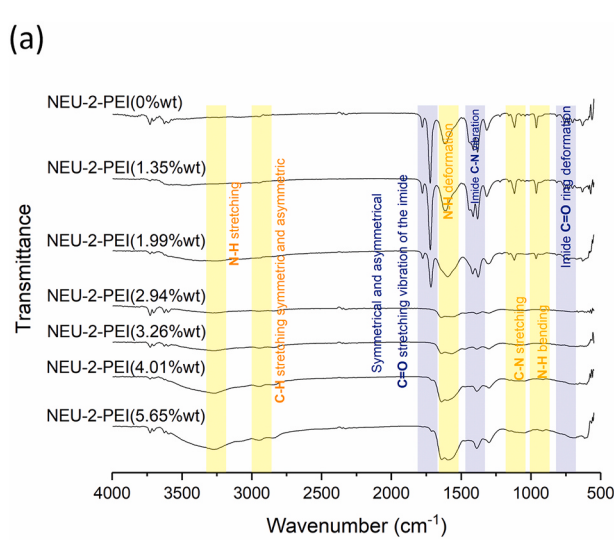


Fig. 4. (a) FTIR spectra of NEU-2-PEI(0%wt), NEU-2-PEI(1.35%wt), NEU-2-PEI(1.99%wt), NEU-2-PEI(2.94%wt), NEU-2-PEI(3.26%wt), NEU-2-PEI(4.01%wt) and NEU-2-PEI(5.65%wt), respectively. (b) Total CO_2 uptake capacity, CO_2 capture capacity in the pseudo-kinetic and pseudo-diffusive regimes and amine efficiency data obtained on the NEU-2 sorbent upon amine loading. The red solid line shows the maximum theoretical amine efficiency of 0.5. The black dashed, red dashed, blue dashed and green dashed lines represent the tendency of total CO_2 uptake capacity, amine efficiency, CO_2 capture capacity in the pseudo-kinetic and pseudo-diffusive regimes upon amine loading, respectively. (For interpretation of the references to colour in this figure legend, the reader is referred to the Web version of this article.)

In other words, the diffusion resistance present within the pores of the material are measured by comparing the fast up-take at the beginning of the capture (pseudo-kinetic regime) to the slow uptake at the end of capture towards equilibrium (pseudo-diffusive regime). The CO₂ uptake capacity in the pseudo-kinetic regime progressively decreased with increasing amine content. On the other hand, the CO₂ capture capacity in the pseudo-diffusive regime increased proportionally with total CO₂ uptake upon amine loading.

3.2.2. Effect of temperature

Fig. 5a shows the effect of temperature on CO₂ uptake for NEU-2-PEI (5.65%wt). The CO₂ uptake capacity decreased significantly as the temperature rises from 25 °C to 75 °C. The increase of temperature (energy) favored gas diffusion and, therefore, reduced the CO₂ sorption. In other words, the higher sorption temperature caused CO₂ to escape the amine during the adsorption process. In addition, high temperatures might have caused the evaporation and/or degradation of PEI within porous NEU-2, thus decreasing CO₂ uptake capacity. Logically, the CO₂ uptake capacity in the pseudo-kinetic regime increased as temperature went from 25 °C to 75 °C. However, the CO₂ capture capacity in the pseudo-diffusive regime decreased proportionally with total CO₂ uptake as the temperature raised. A high uptake temperature was found to reduce the amine efficiency, demonstrating the practicality of utilizing a relatively low temperature sorption supported-amine system to capture CO₂.

The structural alterations in NEU-2-PEI(5.65%wt) due to temperature modification were assessed based on FTIR data (Fig. S15). Both, absorption frequency and intensity did not change. Therefore, NEU-2-PEI(5.65%wt) did not suffer structural alterations upon temperature raising. On the other hand, TEM was performed to test the morphological transformations in NEU-2-PEI(5.65%wt) due to temperature modification. No change in the size or shape of the material was found and, consequently, the overall morphology of NEU-2-PEI(5.65%wt) was maintained upon temperature raising (Fig. S13).

3.2.3. Regeneration

The regenerability of a sorbent is defined as the degree of change in the uptake capacity over multiple cycles of sorption and desorption. The stability and performance over recurring sorption/desorption cycles is a critical indicator for testing a sorbent. Ten adsorption-desorption cyclic experiments were conducted to test the regeneration of NEU-2-PEI (5.65%wt) at 25 °C (Fig. 5b). The equilibrium adsorption capacity value showed a slight decrease after first cycle, which might have been caused

by loss of CO₂ uptake sites due to the misplacing of physically adsorbed amines in the support. After first cycle, the equilibrium adsorption capacity for NEU-2-PEI(5.65%wt) was 0.63 mmol g⁻¹, representing 79.06% of the fresh sorbent. Subsequent cycles (from 2 to 9) display no noticeable loss of sorption capacity. Therefore, NEU-2 was proved to be very stable over 9 cycles. The uptake capacity of NEU-2-PEI(5.65%wt) decreased from 0.61 mmol g⁻¹ to 0.55 mmol g⁻¹ in the last cycle, representing 69.35% of the fresh sorbent. This loss in the adsorption capacity was related to PEI-volatilization within porous NEU-2. The CO₂ uptake capacity in the pseudo-kinetic regime was found to be constant over sorption/desorption cycles. However, the capture capacity in the pseudo-diffusive regime as well as the amine efficiency decreased proportionally with total CO₂ uptake. Therefore, the loss of sorption capacity was related to physical modification, volatilization and/or degradation of PEI but NEU-2 support did not change over multiple cycles of sorption and desorption.

FTIR data were used to assess the structural alterations in NEU-2-PEI (5.65%wt) at 25 °C over recurring sorption/desorption cycles (Fig. S16). Neither adsorption frequency nor intensity changed. Therefore, NEU-2-PEI(5.65%wt) at 25 °C did not suffer structural alterations over multiple cycles of sorption and desorption. TEM was performed to test the morphological modifications in NEU-2-PEI(5.65%wt) at 25 °C due to ten adsorption–desorption cyclic experiments. No change in the size or shape of the material was found and, consequently, the overall morphology of NEU-2-PEI(5.65%wt) at 25 °C was maintained (Fig. S14).

3.2.4. Amorphous versus crystalline metal organic frameworks for adsorptive gas separation

In order to design an efficient MOF for CO₂ capture, it is important to understand MOF structure-property-relationship. Herein, we compared the CO₂ capture capacity of amorphous NEU-2 with our previously created material: crystalline NEU-1c (Fig. S4-7, S20-22, Tables S2 and S6). NEU-2 and NEU-1c present different metal centers (iron and zinc respectively). Both metal nodes display an octahedral coordination environment and same local molecular structure of metal within the MOF. It is worth mentioning that isostructural MOFs with the metal center of lighter atomic weight usually adsorb slightly more CO₂ (Table S7) [81,82]. Accordingly, it could be expected that NEU-1c would have higher CO₂ capture capacity than NEU-2 but it does not. This unforeseen result may be related to the phases of NEU-1c and NEU-2: crystalline *versus* amorphous. MOF size also may affect the CO₂ uptake, larger MOFs usually increase mass transfer resistance [83]. Thus, in terms of particle size, it was anticipated that NEU-2 would have

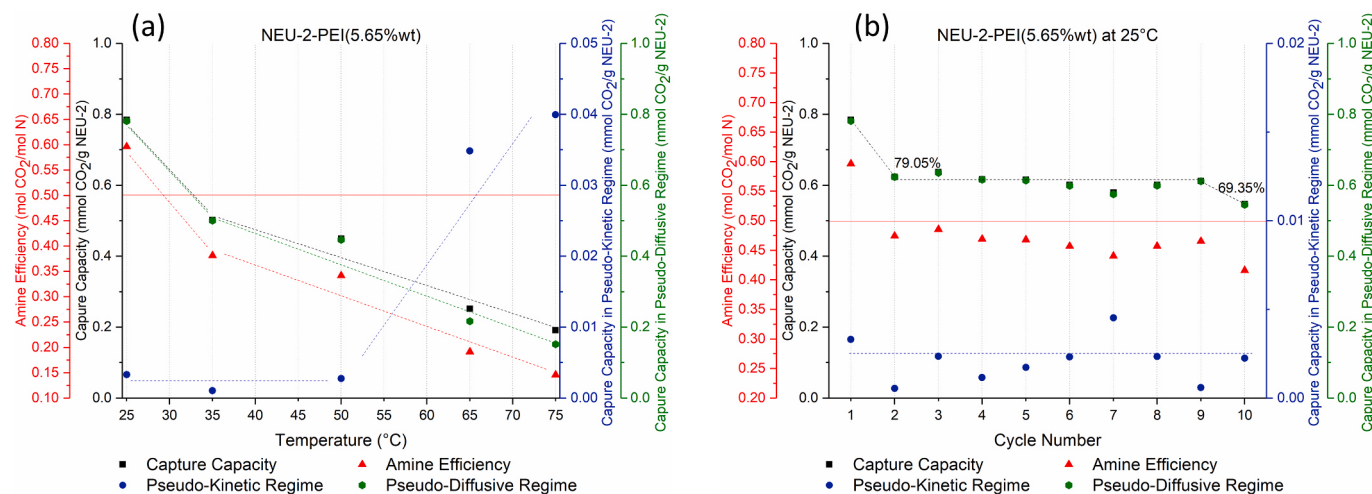


Fig. 5. (a) Total CO₂ uptake capacity, CO₂ capture capacity in the pseudo-kinetic and pseudo-diffusive regimes and amine efficiency data obtained on the NEU-2-PEI (5.65%wt) upon temperature raising. (b) Total CO₂ uptake capacity, CO₂ capture capacity in the pseudo-kinetic and pseudo-diffusive regimes and amine efficiency data obtained on the NEU-2-PEI(5.65%wt) at 25 °C over multiple cycles of sorption and desorption.

higher CO₂ capture capacity than NEU-1, as it happens. The physico-chemical properties of the organic ligand also affect the CO₂ uptake. Here, NEU-2 and NEU-1c are made from H₂BPDI and, therefore, the effect of the organic ligand in CO₂ uptake is exactly alike in the two MOFs. Interestingly, H₂BPDI possesses 4 amide groups. This functional group affords strong CO₂ binding affinity [84]. Amide groups exhibit two types of donor-acceptor affinity sites: (1) the -C=O group and (2) the -NH moiety. The former acts as an electron donor (Lewis base) allowing to establish NC=O...CO₂ interactions; the latter acts as an electron acceptor (Lewis acid) and allows to form NH...OCO interactions [85]. Therefore, H₂BPDI is a promising ligand to fabricate crystalline or amorphous MOFs with large surface area to address the challenge of CO₂ rising. Textural properties (surface area, pore volume and pore size distribution), which also affect the CO₂ capture, are similar in both MOFs (Figs. 3, S20, S21). Beyond the effect of the above-mentioned parameters, the CO₂ capture is also influenced by the forms of NEU-1c and NEU-2: crystalline *versus* amorphous. According to our results and in contrast to what has been stated so far, the ordered crystalline state of MOFs is not a requirement for gas uptake. Novel aMOFs with hierarchical porosity are promising materials for CO₂-capture applications.

Fig. 6 presents the CO₂ capacity *versus* amine weight percent for crystalline NEU-1c and amorphous NEU-2 (detailed in section 3.2.1.). While NEU-1c showed a CO₂ capture capacity of 0.07 mmol g⁻¹ at room temperature in pure CO₂, NEU-2 exhibits an uptake capacity of 0.1136 mmol g⁻¹ under the same conditions. In addition, amorphous NEU-2 can be considered as superior support for amine immobilization as shown in Fig. 6. The flexibility of aMOFs may lead to adaptable behavior towards both amine loading and CO₂ capture. In this context, it can be imagined that the porosity generated into amorphous materials would be dynamic, in contrast to their crystalline counterparts. Hence, unique amorphous NEU-2 may facilitate a variety of chemical separations due to its framework flexibility and, ultimately, its guest-responsive capability.

4. Conclusions

An amorphous iron MOF (Fe(BPDI)Py₂ = NEU-2) was created by using a high electron-donating solvent and a complementary co-solvent to cushion basicity. NEU-2 displayed a hierarchical pore distribution with the presence of micropores, mesopores, and macropores. This multichannel porous aMOF was tested as class 1 sorbent by incorporating large PEI molecules into the mesopores and macropores. The amine density within the system was increased to examine not only the variations in the CO₂ uptake capacity at equilibrium but also the capture capacity in the pseudo-kinetic and pseudo-diffusive regimes and the amine efficiency of the NEU-2-PEI. The results of the NEU-2 scaffold tests showed that CO₂ can access all available amine sites at increasing amine loadings, and therefore the pores were not become blocked resulting in diffusion resistance. Consequently, our multi-channel porous NEU-2 addressed the trade-off between amine loading and low access to amine sites. Tests at different temperatures showed that the CO₂ uptake capacity decreased significantly as the temperature raised from 25 °C to 75 °C. While the CO₂ uptake capacity in the pseudo-kinetic regime increased as temperature went from 25 °C to 75 °C, the CO₂ capture capacity in the pseudo-diffusive regime decreased proportionally with total CO₂ uptake. In addition, a high uptake temperature was found to reduce the amine efficiency. Therefore, it was demonstrated the practicality of utilizing a relatively low temperature sorption supported-amine system to capture CO₂. Furthermore, ten adsorption-desorption cyclic experiments were conducted to test the regeneration of NEU-2-PEI (5.65%wt) at 25 °C. NEU-2 was proved to be very stable over 9 cycles. The loss of sorption capacity was related to physical modification, volatilization and/or degradation of PEI. However, NEU-2 support did not change over multiple cycles of sorption and desorption. Herein, it was also reported a comparative study of the CO₂ capture capacity of amorphous NEU-2 and crystalline NEU-1c. This research demonstrates

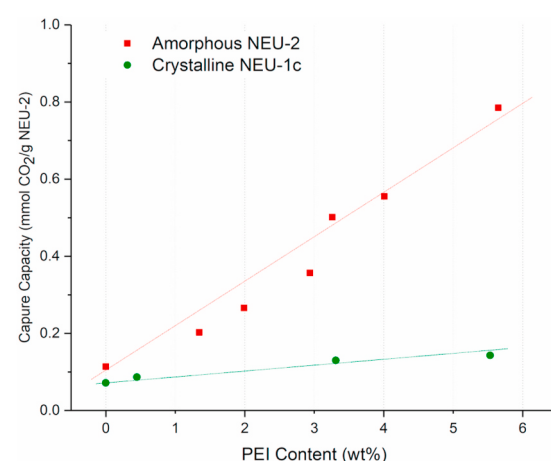


Fig. 6. Comparative study: CO₂ uptake capacity of amorphous NEU-2 and crystalline NEU-1c upon amine loading.

that the ordered crystalline state of MOFs is not a requirement for gas uptake, establishing novel aMOFs with hierarchical porosity as promising materials for CO₂-capture applications.

CRediT authorship contribution statement

Javier Fonseca: conceived and designed experiments, conducted the experiments and performed the data analysis and interpretations, aggregated the figures and wrote the manuscript. All authors discussed the results, drew conclusions and commented on the manuscript. **Sunho Choi:** discussed the applicability of NEU-2 and supervised the work. All authors discussed the results, drew conclusions and commented on the manuscript.

Declaration of competing interest

The authors declare that they have no known competing financial interests or personal relationships that could have appeared to influence the work reported in this paper.

Acknowledgements

This work was supported by the Chemical Engineering Department at Northeastern University. The authors acknowledge for the use of Beamline ISS 7-ID of the National Synchrotron Light Source (NSLS) II. The authors would also like to acknowledge Dr. Sanjeev Mukerjee and William Fowle for the use of his facilities in the analysis of the XRD and TEM/SEM data, respectively. J.F. acknowledges help from Tenghua Gong and Erin Blackley from Northeastern University.

Appendix A. Supplementary data

Supplementary data to this article can be found online at <https://doi.org/10.1016/j.micromeso.2020.110600>.

Funding sources

This research did not receive any specific grant from funding agencies in the public, commercial, or not-for-profit sectors.

¹H NMR spectra, FTIR spectra and DSC of H₂BPDI. X-ray diffraction, X-ray absorption spectra, FTIR spectra, TEM and SEM images, TGA and EDX characterizations, Nitrogen adsorption/desorption isotherms, DFT pore analysis, CO₂ capture trials, and EXAFS fitting results.

References

- [1] Climate change indicators: greenhouse gases. <https://www.epa.gov/climate-indicators/greenhouse-gases>. (Accessed 15 April 2020).
- [2] NASA Earth observatory. <https://earthobservatory.nasa.gov/world-of-change/DecadalTemp>. (Accessed 15 April 2020).
- [3] G.T. Rochelle, Science 325 (2009) 1652–1654, <https://doi.org/10.1126/science.1176731>.
- [4] R. Muraleedharan, A. Mondal, B. Mandal, Separ. Purif. Technol. 94 (2012) 92–96, <https://doi.org/10.1016/j.seppur.2011.10.035>.
- [5] H. Mohamed, K. Johari, A. Mohd, Fuel 232 (2018) 454–462, <https://doi.org/10.1016/j.fuel.2018.06.010>.
- [6] J. Wei, S. Zhao, Adv. Mater. Res. 541 (2012) 2240–2245, <https://doi.org/10.4028/www.scientific.net/AMR.538-541.2240>.
- [7] C.F. Martín, M.G. Plaza, J.J. Pis, F. Rubiera, C. Pevida, T.A. Centeno, Separ. Purif. Technol. 74 (2010) 225–229, <https://doi.org/10.1016/j.seppur.2010.06.009>.
- [8] P. Mishra, S. Mekala, F. Dreisbach, B. Mandal, S. Gumma, Separ. Purif. Technol. 94 (2012) 124–130, <https://doi.org/10.1016/j.seppur.2011.09.041>.
- [9] A. Basile, A. Iulianelli, F. Galluccio, P. Morrone, Developments and innovation in carbon dioxide (CO₂) capture and storage technology. <https://doi.org/10.1533/9781845699574.2.203>, 2010, 203–242.
- [10] M. Vinoba, M. Bhagiyalakshmi, Y. Alqaheem, A.A. Alomair, A. Pérez, M.S. Rana, Separ. Purif. Technol. 188 (2017) 431–450, <https://doi.org/10.1016/j.seppur.2017.07.051>.
- [11] G. Xu, F. Liang, Y. Yang, Y. Hu, K. Zhang, W. Liu, Energies (2014) 3484–3502, <https://doi.org/10.3390/en7053484>.
- [12] M. Rong, L. Yang, L. Wang, J. Yu, H. Qu, H. Liu, J. Colloid Interface Sci. 548 (2019) 265–274, <https://doi.org/10.1016/j.jcis.2019.04.036>.
- [13] H. Mohamed, A. Mohd, K. Johari, Separ. Purif. Technol. 222 (2019) 297–308, <https://doi.org/10.1016/j.seppur.2019.04.029>.
- [14] X. Wang, W. Zeng, M. Song, F. Wang, X. Hu, Q. Guo, Y. Liu, Chem. Eng. J. 364 (2019) 475–484, <https://doi.org/10.1016/j.cej.2019.02.008>.
- [15] H.T. Kwon, M.A. Sakwa-Novak, S.H. Pang, A.R. Sujan, E.W. Ping, C.W. Jones, Chem. Mater. 31 (2019) 5229–5237, <https://doi.org/10.1021/acs.chemmater.9b01474>.
- [16] W. Wang, J. Motuzas, X.S. Zhao, J.C. Diniz da Costa, Separ. Purif. Technol. 222 (2019) 381–389, <https://doi.org/10.1016/j.seppur.2019.04.050>.
- [17] W. Wang, J. Motuzas, X.S. Zhao, J.C. Diniz da Costa, Ind. Eng. Chem. Res. 57 (2018) 5653–5660, <https://doi.org/10.1021/acs.iecr.8b00129>.
- [18] L.A. Darunte, Y. Terada, C.R. Murdock, K.S. Walton, D.S. Sholl, C.W. Jones, ACS Appl. Mater. Interfaces 2 (2017) 17042–17050, <https://doi.org/10.1021/acsmami.7b02035>.
- [19] Y. Lin, C. Kong, L. Chen, RSC Adv. 6 (2016) 32598–32614, <https://doi.org/10.1039/c6ra01536k>.
- [20] T.M. McDonald, J.A. Mason, X. Kong, E.D. Bloch, D. Gygi, A. Dani, V. Crocella, F. Giordanino, S.O. Odoh, W.S. Drisdell, B. Vlaisavljevich, A.L. Dzubak, R. Poloni, S.K. Schnell, N. Planas, K. Lee, T. Pascal, L.F. Wan, D. Prendergast, J.B. Neaton, B. Smit, J.B. Kortright, L. Gagliardi, S. Bordiga, J.A. Reimer, J.R. Long, Nature 519 (2015) 303–308, <https://doi.org/10.1038/nature14327>.
- [21] T.D. Bennett, A.K. Cheetham, Acc. Chem. Res. 47 (2014) 1555–1562, <https://doi.org/10.1021/ar5000314>.
- [22] T.D. Bennett, S. Horike, Nat. Rev. Mater. 3 (2018) 431–440, <https://doi.org/10.1038/s41578-018-0054-3>.
- [23] J.M. Tuffnell, C.W. Ashling, J. Hou, S. Li, L. Longley, M.L. Ríos Gómez, T. D. Bennett, Chem. Commun. (J. Chem. Soc. Sect. D) 55 (2019) 8705–8715, <https://doi.org/10.1039/C9CC01468C>.
- [24] T.D. Bennett, A.L. Goodwin, M.T. Dove, D.A. Keen, M.G. Tucker, E.R. Barney, A. K. Soper, E.G. Bithell, J.-C. Tan, A.K. Cheetham, Phys. Rev. Lett. 104 (2010) 1–4, <https://doi.org/10.1103/PhysRevLett.104.115503>.
- [25] T.D. Bennett, D.A. Keen, J.-C. Tan, E.R. Barney, A.L. Goodwin, A.K. Cheetham, Angew. Chem. Int. Ed. 50 (2011) 3067–3071, <https://doi.org/10.1002/anie.201007303>.
- [26] K. Ohara, J. Martí-Rujas, T. Haneda, M. Kawano, D. Hashizume, F. Izumi, M. Fujita, J. Am. Chem. Soc. 131 (2009) 3860–3861, <https://doi.org/10.1021/ja9005145>.
- [27] H. Ohtsu, T.D. Bennett, T. Kojima, D.A. Keen, Y. Niwa, M. Kawano, Chem. Commun. (J. Chem. Soc. Sect. D) 53 (2017) 7060–7063, <https://doi.org/10.1039/C7CC03333H>.
- [28] J. Martí-Rujas, N. Islam, D. Hashizume, F. Izumi, M. Fujita, M. Kawano, J. Am. Chem. Soc. 133 (2011) 5853–5860, <https://doi.org/10.1021/ja109160a>.
- [29] J.-W. Xiu, G.-E. Wang, M.-S. Yao, C.-C. Yang, C.-H. Lin, G. Xu, Chem. Commun. 53 (2017) 2479–2482, <https://doi.org/10.1039/C6CC09310H>.
- [30] X. Zhang, H. Li, X. Lv, J. Xu, Y. Wang, C. He, N. Liu, Y. Yang, Y. Wang, Chem. Eur. J. 24 (2018) 8822–8832, <https://doi.org/10.1002/chem.201800773>.
- [31] N. Masciocchi, G.A. Ardizzone, G. LaMonica, A. Maspero, S. Galli, A. Sironi, Inorg. Chem. 40 (2001) 6983–6989, <https://doi.org/10.1021/ic010585d>.
- [32] N. Masciocchi, S. Bruni, E. Cariati, F. Cariati, S. Galli, A. Sironi, Inorg. Chem. 40 (2001) 5897–5905, <https://doi.org/10.1021/ic010384>.
- [33] H. Zhou, M. Zheng, H. Tang, B. Xu, Y. Tang, H. Pang, Small 16 (2020) 1–9, <https://doi.org/10.1002/smll.201904252>.
- [34] C. Orellana-Tavra, M. Köppen, A. Li, N. Stock, D. Fairen-Jimenez, ACS Appl. Mater. Interfaces 12 (2020) 5633–5641, <https://doi.org/10.1021/acsami.9b21692>.
- [35] A. Kertik, L.H. Wee, M. Pfannmöller, S. Bals, J.A. Martens, I.F.J. Vankelecom, Energy Environ. Sci. 10 (2017) 2342–2351, <https://doi.org/10.1039/C7EE01872J>.
- [36] T.D. Bennett, P. Simoncic, S.A. Moggach, F. Gozzo, P. Macchi, D.A. Keen, J.-C. Tan, A.K. Cheetham, Chem. Commun. 47 (2011) 7983–7985, <https://doi.org/10.1039/c1cc11985k>.
- [37] K.W. Chapman, G.J. Halder, P.J. Chupas, J. Am. Chem. Soc. 131 (2009) 17546–17547, <https://doi.org/10.1021/ja908415z>.
- [38] Y.H. Hu, L. Zhang, Phys. Rev. B 81 (2010) 1–5, <https://doi.org/10.1103/PhysRevB.81.174103>.
- [39] K.W. Chapman, D.F. Sava, G.J. Halder, P.J. Chupas, T.M. Nenoff, J. Am. Chem. Soc. 133 (2011) 18583–18585, <https://doi.org/10.1021/ja2085096>.
- [40] Y. Hu, H. Kazemian, S. Rohani, Y. Huang, Y. Song, Chem. Commun. 47 (2011) 12694–12696, <https://doi.org/10.1039/C1CC15525C>.
- [41] A.J. Graham, A.-M. Banu, T. Düren, A. Greenaway, S.C. McKellar, J.P.S. Mowat, K. Ward, P.A. Wright, S.A. Moggach, J. Am. Chem. Soc. 136 (2014) 8606–8613, <https://doi.org/10.1021/ja411934f>.
- [42] Z. Su, Y.-R. Miao, S.-M. Mao, G.-H. Zhang, S. Dillon, J.T. Miller, K.S. Suslick, J. Am. Chem. Soc. 137 (2015) 1750–1753, <https://doi.org/10.1021/ja5113436>.
- [43] S.H. Lapidus, G.J. Halder, P.J. Chupas, K.W. Chapman, J. Am. Chem. Soc. 135 (2013) 7621–7628, <https://doi.org/10.1021/ja4012707>.
- [44] A.J. Graham, A.-M. Banu, T. Düren, A. Greenaway, S.C. McKellar, J.P.S. Mowat, K. Ward, P.A. Wright, S.A. Moggach, J. Am. Chem. Soc. 136 (2014) 8606–8613, <https://doi.org/10.1021/ja411934f>.
- [45] R. Zacharia, D. Cossement, L. Lafi, R. Chahine, J. Mater. Chem. 20 (2010) 2145–2151, <https://doi.org/10.1039/B922991D>.
- [46] Y. Zhou, C. Liu, Plasma Chem. Plasma Process. 31 (2011) 499–506, <https://doi.org/10.1007/s11090-011-9290-7>.
- [47] T.D. Bennett, S. Cao, J.C. Tan, D.A. Keen, E.G. Bithell, P.J. Beldon, T. Friscic, A. K. Cheetham, J. Am. Chem. Soc. 133 (2011) 14546–14549, <https://doi.org/10.1021/ja206082s>.
- [48] S. Cao, T.D. Bennett, D.A. Keen, A.L. Goodwin, A.K. Cheetham, Chem. Commun. 48 (2012) 7805–7807, <https://doi.org/10.1039/c2cc33773h>.
- [49] T.D. Bennett, P.J. Saines, D.A. Keen, J.-C. Tan, A.K. Cheetham, Chem. Eur. J. 19 (2013) 7049–7055, <https://doi.org/10.1002/chem.201300216>.
- [50] C. Orellana-Tavra, E.F. Baxter, T. Tian, T.D. Bennett, N.K.H. Slater, A.K. Cheetham, D. Fairen-Jimenez, Chem. Commun. 51 (2015) 13878–13881, <https://doi.org/10.1039/c5cc05237h>.
- [51] T. Panda, S. Horike, K. Hagi, N. Ogiwara, K. Kadota, T. Itakura, M. Tsujimoto, S. Kitagawa, Angew. Chem. Int. Ed. 56 (2017) 2413–2417, <https://doi.org/10.1002/ange.201612587>.
- [52] X. Wu, H. Yue, Y. Zhang, X. Gao, X. Li, L. Wang, Y. Cao, M. Hou, H. An, L. Zhang, S. Li, J. Ma, H. Lin, Y. Fu, H. Gu, W. Lou, W. Wei, R.N. Zare, J. Ge, Nat. Commun. 10 (2019) 1–8, <https://doi.org/10.1038/s41467-019-13153-x>.
- [53] L. Zou, C.-C. Hou, Z. Liu, H. Pang, Q. Xu, J. Am. Chem. Soc. 140 (2018) 15393–15401, <https://doi.org/10.1021/jacs.8b00902>.
- [54] B. Li, H.C. Zeng, Chem. Mater. 31 (2019) 5320–5330, <https://doi.org/10.1021/acs.chemmater.9b02070>.
- [55] M.R. Lohe, M. Rose, S. Kaskel, Chem. Commun. 40 (2009) 6056–6058, <https://doi.org/10.1039/b910175f>.
- [56] Z. Xin, X. Chen, Q. Wang, Q. Chen, Q. Zhang, Microporous Mesoporous Mater. 169 (2013) 218–221, <https://doi.org/10.1016/j.micromeso.2012.11.003>.
- [57] J. Ma, X. Bai, W. He, S. Wang, L. Li, H. Chen, T. Wang, X. Zhang, Y. Li, L. Zhang, J. Chen, F. Meng, Y. Fu, Chem. Commun. 55 (2019) 12567–12570, <https://doi.org/10.1039/C9CC06109F>.
- [58] T. Zhang, J. Wang, W. Zhang, C. Yang, L. Zhang, W. Zhu, J. Sun, G. Li, T. Li, J. Wang, J. Mater. Chem. 7 (2019) 2845–2854, <https://doi.org/10.1039/C8TA10394A>.
- [59] R.-Z. Zhang, S. Quan, M. Xia, Q. Wang, W. Zhang, J.-M. Yang, J. Colloid Interface Sci. 525 (2018) 54–61, <https://doi.org/10.1016/j.jcis.2018.04.039>.
- [60] X. Cui, L. Zhang, J. Zhang, L. Gong, M. Gao, P. Zheng, L. Xiang, W. Wang, W. Hu, Q. Xu, W. Wei, H. Zeng, Nanomater. Energy 59 (2019) 102–109, <https://doi.org/10.1016/j.nanoen.2019.02.034>.
- [61] M. Marmier, M.D. Wise, J.J. Holstein, P. Pattison, K. Schenk, E. Solari, R. Scopelliti, K. Severin, Inorg. Chem. 55 (2016) 4006–4015, <https://doi.org/10.1021/acs.inorgchem.6b00276>.
- [62] T. Ueda, T. Tominaga, T. Mochida, K. Takahashi, S. Kimura, Chem. Eur. J. 24 (2018) 1–4, <https://doi.org/10.1002/chem.201801365>.
- [63] K.M. Elsabawy, A.M. Fallatah, J. Mol. Struct. 1177 (2019) 255–259, <https://doi.org/10.1016/j.molstruc.2018.09.069>.
- [64] M. Zhao, Q. Zhao, J. Qiu, X. Lu, G. Zhang, H. Xue, H. Pang, Part. Part. Syst. Char. 34 (2017) 1–8, <https://doi.org/10.1002/ppsc.201600412>.
- [65] R.P.M. Colodrero, K.E. Papathanasiou, N. Stavgiannoudaki, P. Olivera-Pastor, E. R. Losilla, M.A.G. Aranda, L. León-Reina, J. Sanz, I. Sobrados, D. Choquessillo-Lazarte, J.M. García-Ruiz, P. Atienzar, F. Rey, K.D. Demadis, A. Cabeza, Chem. Mater. 24 (2012) 3780–3792, <https://doi.org/10.1021/cm302381k>.
- [66] T.D. Bennett, J.-C. Tan, Y. Yue, E. Baxter, C. Ducati, N.J. Terrill, H.H.-M. Yeung, Z. Zhou, W. Chen, S. Henke, A.K. Cheetham, G.N. Greaves, Nat. Commun. 6 (2015) 1–7, <https://doi.org/10.1038/ncomms9079>.
- [67] T.D. Bennett, Y. Yue, P. Li, A. Qiao, H. Tao, N.G. Greaves, T. Richards, G. I. Lampronti, S.A.T. Redfern, F. Blanc, O.K. Farha, J.T. Hupp, A.K. Cheetham, D. A. Keen, J. Am. Chem. Soc. 138 (2016) 3484–3492, <https://doi.org/10.1021/jacs.5b13220>.
- [68] A. Qiao, T.D. Bennett, H. Tao, A. Krajnc, G. Mali, C.M. Doherty, A.W. Thornton, J. C. Mauro, G.N. Greaves, Y. Yue, Sci. Adv. 4 (2018) 1–7, <https://doi.org/10.1126/sciadv.aao6827>.
- [69] R. Gaillac, P. Pullumbi, K.A. Beyer, K.W. Chapman, D.A. Keen, T.D. Bennett, F.-X. Couder, Nat. Mater. 16 (2017) 1149–1154, <https://doi.org/10.1038/nmat4998>.
- [70] N. Giri, M.G. Del Pópolo, G. Meliaugh, R.L. Greenaway, K. Rätzke, T. Koschine, L. Pison, M.F. Costa Gomes, A.I. Cooper, S.L. James, Nature 527 (2015) 216–220, <https://doi.org/10.1038/nature16072>.

- [71] K.W. Chapman, D.F. Sava, G.J. Halder, P.J. Chupas, T.M. Nenoff, J. Am. Chem. Soc. 133 (2011) 18583–18585, <https://doi.org/10.1021/ja2085096>.
- [72] N. Barooah, R.J. Sarma, J.B. Baruah, CrystEngComm 8 (2006) 608–615, <https://doi.org/10.1039/b607323a>.
- [73] C.-H. Ge, X.-D. Zhang, H.-D. Zhang, Y. Zhao, X.-Q. Li, R. Zang, Mol. Cryst. Liq. Cryst. 534 (2011) 114–123, <https://doi.org/10.1080/15421406.2010.526532>.
- [74] J. Fonseca, S. Choi, Inorg. Chem. 59 (2020) 3983–3992, <https://doi.org/10.1021/acs.inorgchem.9b03667>.
- [75] B. Ravel, M. Newville, J. Synchrotron Radiat. 12 (2005) 537–541, <https://doi.org/10.1107/S0909049505012719>.
- [76] E.J. Baerends, D.E. Ellis, P. Ros, Chem. Phys. 2 (1973) 41–51, [https://doi.org/10.1016/0301-0104\(73\)80059-X](https://doi.org/10.1016/0301-0104(73)80059-X).
- [77] E.J. Baerends, P. Ros, Chem. Phys. 8 (1975) 412–418, [https://doi.org/10.1016/0301-0104\(75\)80152-2](https://doi.org/10.1016/0301-0104(75)80152-2).
- [78] C. Fonseca-Guerra, J.G. Snijders, G. te Velde, E.J. Baerends, Theor. Chem. Acc. 99 (1998) 391–403, <https://doi.org/10.1007/s002140050353>.
- [79] H. Wu, Y. Chen, D. Lv, R. Shi, Y. Chen, Z. Li, Q. Xia, Separ. Purif. Technol. 212 (2019) 51–56, <https://doi.org/10.1016/j.seppur.2018.11.005>.
- [80] X. Zhang, L. Hou, B. Liu, L. Cui, Y.-Y. Wang, B. Wu, Cryst. Growth Des. 13 (2013) 3177–3187, <https://doi.org/10.1021/cg400579w>.
- [81] S.-L. Huang, L. Zhang, Y.-J. Lin, G.-X. Jin, CrystEngComm 15 (2013) 78–85, <https://doi.org/10.1039/C2CE26072G>.
- [82] A.O. Yazaydin, R.Q. Snurr, T.-H. Park, K. Koh, J. Liu, M.D. Levan, A.I. Benin, P. Jakubczak, M. Lanuza, D.B. Galloway, J.J. Low, R.R. Willis, J. Am. Chem. Soc. 131 (2009) 18198–18199, <https://doi.org/10.1021/ja9057234>.
- [83] D. Andirova, C.F. Cogswell, Y. Lei, S. Choi, Microporous Mesoporous Mater. 219 (2016) 276–305, <https://doi.org/10.1016/j.micromeso.2015.07.029>.
- [84] B. Zheng, H. Liu, Z. Wang, X. Yu, P. Yi, J. Bai, CrystEngComm 15 (2013) 3517–3520, <https://doi.org/10.1039/C3CE26177H>.
- [85] V. Safarifard, S. Rodríguez-Hermida, V. Guillerm, I. Imaz, M. Bigdeli, A. Azhdari Tehrani, J. Juanhuix, A. Morsali, M.E. Casco, J. Silvestre-Albero, E.V. Ramos-Fernandez, D. MasPOCH, Cryst. Growth Des. 16 (2016) 6016–6023, <https://doi.org/10.1021/acs.cgd.6b01054>.